

# MEASUREMENT OF SURFACE DISPLACEMENT CAUSED BY UNDERGROUND NUCLEAR EXPLOSIONS BY DIFFERENTIAL SAR INTERFEROMETRY

X. Cong<sup>a</sup>, KH. Gutjahr<sup>b</sup>, J. Schlittenhardt<sup>a</sup>, U. Soergel<sup>c</sup>,

<sup>a</sup> Bundesanstalt für Geowissenschaften und Rohstoffe (BGR), Stilleweg 2, 30655 Hannover – Xiaoying.Cong@bgr.de, J.Schlittenhardt@bgr.de

<sup>b</sup> Institute of Digital Image Processing, Joanneum Research Forschungsgesellschaft mbH, Wastiangasse 6, 8010 Graz, Austria – karlheinz.gutjahr@joanneum.at

<sup>c</sup> Institute of Photogrammetry and GeoInformation, Leibniz University Hannover, Nienburger Str. 1, 30167 Hannover, Germany – soergel@ipi.uni-hannover.de

## Commission VII

**KEY WORDS:** Differential SAR Interferometry, Underground Nuclear Test, Nevada Test Site, Surface Deformation Monitoring, CTBT

### ABSTRACT:

Differential synthetic aperture radar Interferometry (DInSAR) has nowadays become an important means for measuring and monitoring of surface displacements of various types. This paper focuses on investigating the capability of this technique for detection and characterization of past underground nuclear explosions at the Nevada Test Site (NTS), especially the synergy with seismic data. By this analysis large scale surface subsidence phenomena were revealed, which were either related to the detonation itself or post-event deformation. Data of different kinds, namely satellite data from both ERS 1 and 2, external DEM and seismic sources etc., have been used for interferogram processing and interpretation. Because of the date limitation by the first acquired data from NTS, only few test events could be studied coseismically (i.e. from SAR data covering the period before and after the detonation); in the other cases investigations were restricted to postseismic deformation, i.e. restricted to post-event SAR data. The analysis was not limited to determination of the center of gravity of the subsidence crater, but also shape and depth of the deformation pattern were extracted. Theoretically, the amount of deformation could be measured with millimeter accuracy. But in reality, many other error sources must be taken into account, such as atmospheric effects, temporal decorrelation, and noise. Although this accuracy limit is therefore hard to realize in practice, the achieved precision usually outperforms other remote sensing techniques.

This work has been carried out in part within the framework of the Global Monitoring for Security and Stability (GMOSS) Network of Excellence initiated by the European Commission.

## 1. INTRODUCTION

Synthetic Aperture Radar (SAR) uses the microwave domain of the electromagnetic spectrum for remote sensing. Due to the active sensor principle and the long wavelength ranging from a few centimetres to metres, SAR sensors are capable of gathering mapping data independently from weather conditions or time of day. In order to achieve imagery of high spatial resolution besides the signal amplitude the phase data are also acquired. Based on the phase data interferometric processing of several images can be carried out. One standard application for such SAR Interferometry (InSAR) is to derive digital elevation models (DEM) from couples of SAR images taken from different across-track sensor positions. Recent years saw the breakthrough of an extension of InSAR: Differential SAR Interferometry technique using time series of SAR images became an important means for deformation monitoring.

This paper focuses on the application of DInSAR technique to monitor large scale surface subsidence caused by past underground nuclear explosions at Nevada Test Site, (see Figure 1) (Vincent et al, 2003). Five ERS SLC (Single Look Complex) images were analyzed incorporating a given reference SRTM (Shuttle Radar Topography Mission) DEM, which was used to remove phase components induced by topography. By spectral filtering non-overlapping parts of the

image spectra were eliminated before the difference interferograms were calculated. After phase unwrapping the SAR line-of-sight (LOS) velocity vector fields could be derived from these phase differences according to a linear relation. Adding an additional constraint (motion is assumed to consist of vertical subsidence only without any horizontal component) and taking into account the sensor acquisition times subsidence rates can be directly calculated from the LOS vector field. The subsidence rates of coseismic and postseismic signals were finally measured from the geocoded displacement maps.

Based on the given SAR data mainly postseismic subsidence processes could be monitored. The deformation may cover large areas of one kilometer or more in diameter on the surface above the point of explosion. According to the local geological situation the actual point of explosion known from ground-truth may not be located in the centre of deformation area. Therefore, 3D analysis was accomplished, to extract more detailed information about the relation between the position of the test and the subsidence pattern's center of gravity. Since the observed subsidence could be composed by superposition of the effects of several individual tests nearby creating a cluster signal, this effect must be taken into account for the accurate location determination of the test position. By considering the possible variations in the geologic and hydrologic environment of the local test area and taking into account the variance of

individual measurements the results for the derived decay constants and initial deformation rates did not show clear regional distinctions. Furthermore, a continuous sinking sequence was derived from the postseismic signals. The other emphasis will be placed on the data processing and the discussion of the reliability of delivered results.

The research of using DInSAR technique for detecting/monitoring underground nuclear explosion is of relevance for CTBT (Comprehensive Nuclear Test-Ban Treaty) verification regime (Canty & Schlittenhardt, 2001). Special emphasis will be placed on accessing whether signals detected by DInSAR could be used in the CTBT verification scenario in combination with the seismic data.

## 2. DATA PROCESSING AND RESULTS

### 2.1 Nevada Test Site and ERS data

The Nevada Test Site is located in Nye County in southern Nevada about 105 km northwest of the City of Las Vegas, near 37°07'N, 116°03'W. In Figure 1 the site is highlighted with a black polygon. From 1962 to 1992 over 1000 underground nuclear tests were carried out there. The nuclear tests were documented in-situ with on-site-inspection or remotely by seismic and other methods. The red rectangle in Figure 1 represents the area covered by ERS data; the green and blue rectangles depict two prominent areas called Pahute Mesa (PM) and Yucca Flat (YF).

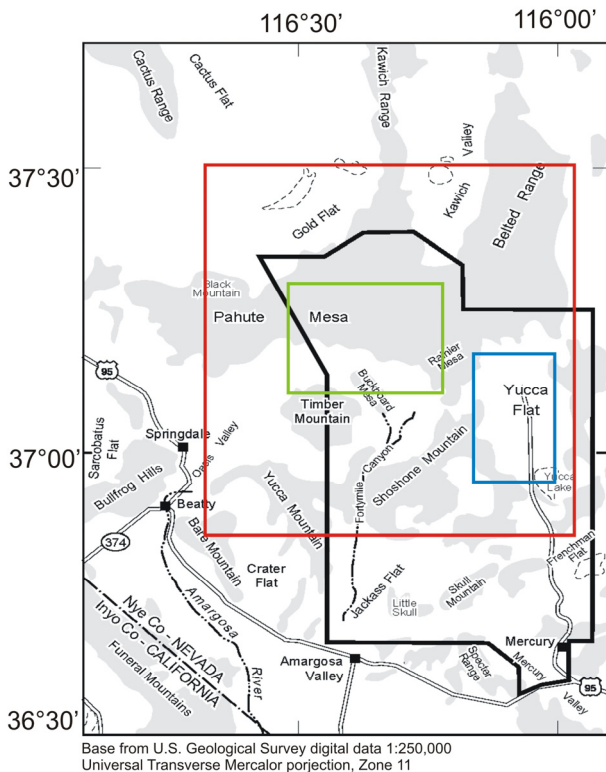


Figure 1. Geographical overview for NTS (black polygon), ERS data (red rectangle), PM area (green), and YF (blue)

The acquisition dates of ERS data available for the processing are shown in Figure 2. First ERS data were taken in 1992 when a moratorium on all U.S. nuclear tests came into effect. Last test “Divider” was conducted on 23. Sep. 1992. The other four tests

that have taken place after the acquisition time of the first ERS scene are located in Yucca Flat, except for Hunters Trophy in Rainier Mesa. The 5 ERS scenes are illustrated in time diagram with the red folded line and the acquisition date, and the data were numbered consecutively with index from 1 to 5. Hence, it is possible that both of coseismic and postseismic signals as well as the long-term deformation signals could be captured.

In addition to the ERS data an external DEM is essential for the processing. The SRTM X-band DEM (30 m resolution) covering the entire area was used here. Moreover, the heterogeneous seismic data were needed for the further interpretation (Springer et al., 2002).

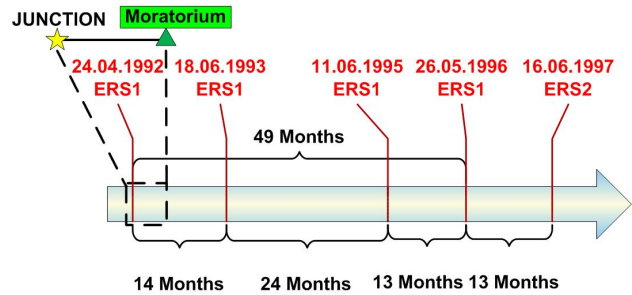


Figure 2. Time diagram of five ERS scenes

### 2.2 Processing with DInSAR method

All the processing steps are carried out using the software package ‘RSG’ which is developed at Joanneum Research (Gutjahr, 2004). The DInSAR processing following the work flow depicted in Figure 3 is carried out in image pairs. Two criteria have been applied for selection of the image pairs. The first was minimization of the perpendicular baseline component, and the second was to obtain orbit pairs of different time spans and epochs in order to acquire versatile deformation signals. Table 1 lists the interferometric orbit pairs along with relevant interferometry parameters.

Image pairs	Sensors	Epoch	Baseline	
			temporal [days]	spatial [m]
1/2	ERS 1	920424-930618	420	-41
2/3	ERS 1	930618-950611	723	-59
3/4	ERS 1	950611-960526	350	18
4/5	ERS 1 & 2	960526-970616	386	-87
3/5	ERS 1	920424-960526	386	-10
1/4	ERS 1	920424-960526	1493	-25
1/5	ERS 1 & 2	960526-970616	1879	-112

Table 1. InSAR orbit pairs and the relevant parameters

Five available ERS images were processed to seven interferograms (Table 1), incorporating the given reference SRTM DEM, which was used to remove phase components induced by topography via phase simulation. By spectral filtering non-overlapping parts of the image spectra were eliminated before the difference interferograms were calculated. After phase unwrapping the SAR line-of-sight (LOS) velocity vector fields can be derived from the difference of real and simulated interferometric phase. According to an additional constraint (assuming only subsidence and no horizontal

movement component) and taking into account the sensor acquisition times the LOS vector field can be directly transformed into vertical subsidence rates. Then the subsidence rates of coseismic and postseismic signals were extracted from the geocoded displacement maps (Figure 3). The deformation signals are given in form of the depth (motion in vertical direction over the time interval of the image pair). Besides depth, the shape of the deformation crater and the location of the estimated center of gravity as auxiliary information were listed in Table 2. During the processing the atmospheric influence was neglected, which is assumed to be small in this arid environment.

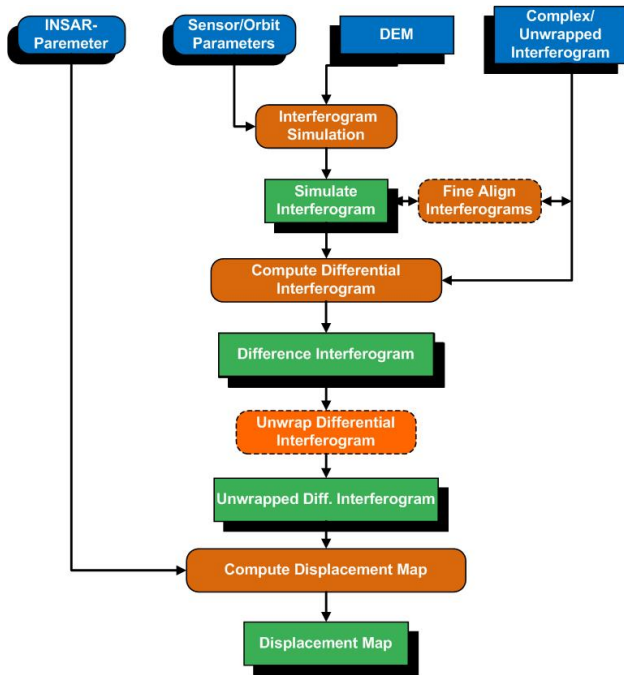


Figure 3. Process sequence of differential SAR interferometry.

### 2.3 Coseismic and postseismic signals

After the differential InSAR processing both coseismic and postseismic signals were derived from the image pairs. From image pair 1/2 coseismic and postseismic signals were extracted with high quality compared to ground truth (Springer et al., 2002).

#### Coseismic signals

Figure 4 shows two coseismic signals from the differential interferogram created using the image pair 1/2. The measured subsidence area center was located in center point of the image, (see Table 3). Galena ( $M_L = 3.9$ ) and Divider ( $M_L = 4.4$ ) formed observable coseismic collapse craters measuring 134 and 122 meters in diameter and 8 and 3 meters in depth. These values exceed by far the unambiguous measurement range in LOS of 2.83 cm of C-band (half of 5.66 cm wavelength). For this reason by using InSAR to capture coseismic signals of this size will lead to loss of information near surface ground zero. On the other hand for the detection of larger deformations (most of them occurred coseismically too) it is more suitable to apply methods which use optical EO data (Canty et al., 2005).

#### Postseismic signals

From the given data mainly postseismic subsidence signals, e.g. all tests in PM were postseismic events, could be obtained. The deformation may extend over large areas of one kilometer or more in diameter on the surface above the point of explosion (Figure 5). According to the local geological situation the actual point of explosion known from ground truth may not be located in the centre of deformation area. Firstly, the data in Springer et al., 2002 were given with accuracy of ca. 100 m, corresponding to a location uncertainty of three pixels. Secondly, consideration of a single exposition might not be sufficient here, because additional deformation processes caused by historical tests nearby can lead to more complex subsidence patterns. In such case the estimated center point could be biased from these superimposed contributions. Thirdly, generalization effects in the SRTM DEM lead to errors both in the phase simulation and in the geocoding step. The mentioned effects caused that in the area existed many peaks side by side. To tackle this problem, the field was analyzed in 3-D, where the deformation signals were included.

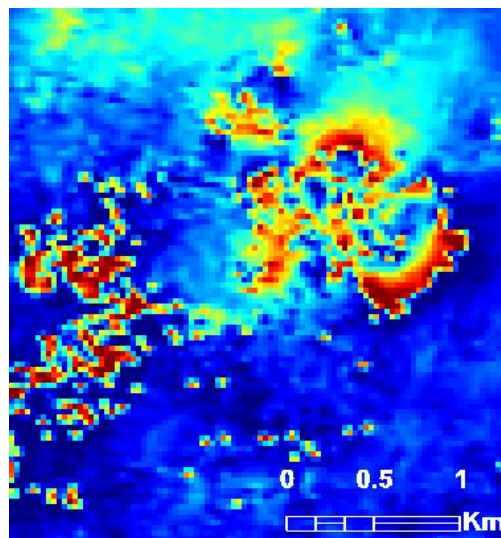
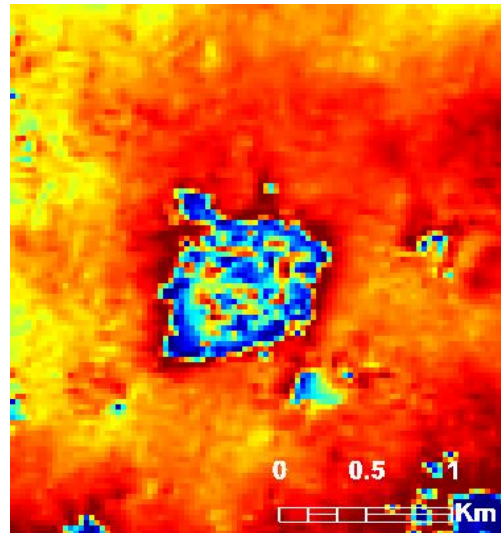


Figure 4. Coseismic deformation signals of two of the last five underground nuclear tests conducted at NTS in 1992 captured by 14 months period InSAR pair 1/2; coseismic events Galena (top) und Divider (bottom).



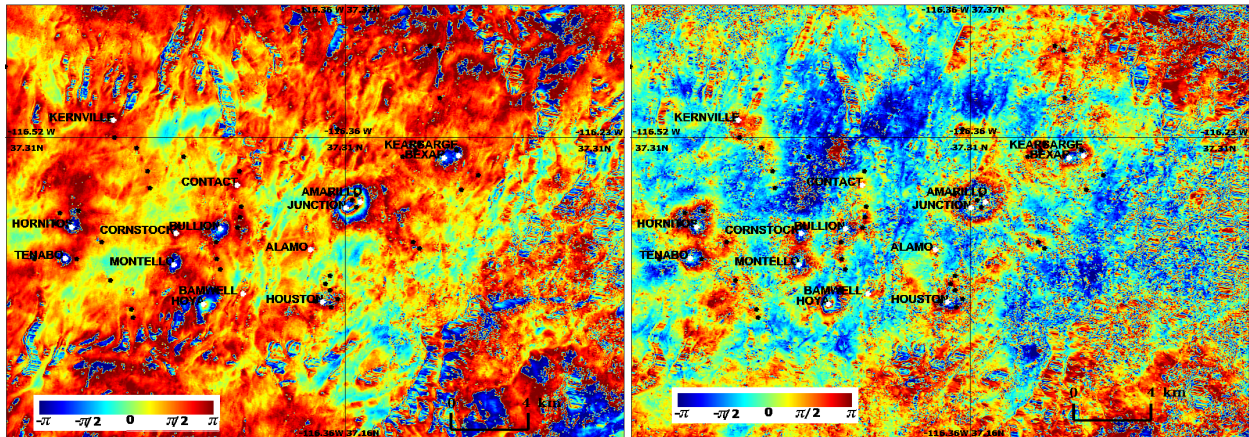


Figure 5. Postseismic surface deformation signals from underground nuclear tests conducted in Pahute Mesa region of NTS (green rectangle in figure 1); the Pair 1/2 (left) spanning 14 months accumulation of deformation und 1/4 (right) spanning 49 months. Larger white dots denote the underground tests after 1988, and the smaller black dots denote the tests from 1975 to 1987.

Test Information				a	b	$\phi$	Center of Ellipse/Circle			Collapse Crater Diameter [m]
Code-Name	Date	Region Code	Magnitude	r [m]		[ $^{\circ}$ ]	Depth [cm]	Latitude [ $^{\circ}$ ]	Longitude [ $^{\circ}$ ]	
Divider	23.09.1992	YF	4.4 M <sub>L</sub>	270.0		--	-3.4	37.018	-115.994	--
Galena	23.06.1992	YF	3.9 M <sub>L</sub>	330.0		--	-4.4	37.125	-116.033	134
Junction	26.03.1992	PM	5.5 M <sub>b</sub>	1044.8	750.6	50.8	-7.0	37.274	-116.359	--

Table 2. Parameters of ellipse (a and b, semi-major and semi-minor axis;  $\phi$ , angle of orientation) or circle (r, radius) and of the deformation center (depth of center, location of center with latitude and longitude) of the three most recent nuclear tests derived from image pair 1/2.

Thereby more information about the relation between the position of the test and the center of movement could be gained. The measured signals were used for the calculation the deformation decay rate of the crater with a simple exponential equation (see Table 2). In Figure 5 both differential interferograms present rather similar situations, actually the deformation decays quite rapidly after one to two years. However, both pairs share the same reference data of 1992. Since the observed subsidence signal could be composed by superposition of the effects of several tests nearby and created by a cluster signal (see Figure 6 left).

### Crater Modelling – Spall zone

Test Junction detonated on 26<sup>th</sup> of March 1992 and it was the last nuclear test to be carried out underground in PM. In Figure 6 images show the interferogram und displacement map from image pair 1/2. The detonation happened about a month before the first ERS image was gathered. Therefore, the captured deformation signals were purely postseismic. Figure 6 (top) illustrates five tests (black and white dots) including Junction inside of the deformation area, and one test just outside of it. The areas with significant deformations could be related to many explosions inside the area, but it is more expedient to label the area with a unique name. Accurately the measured deformation was a clustering signal composed by the complex motion. According to the spall zone modelling the deformation decayed rapidly with time. Therefore, the effects of detonations before the year 1988 could be neglected compared to the later ones. Then the distance from the deformation center was taken into account. The detected subsidence area indicated an

elliptical deformation pattern, the semi major and semi minor axes of approximately 1.0 and 0.8 km, whose parameters are given in Table 2. Figure 6 (bottom) also shows the vertical profile across the deformation centre. For the determination of the depth of the subsidence, first a local reference level was estimated from the data in order to eliminate systematic effects; then the depth 'd' was measured from the deepest point along the profile to this reference surface. The measured radius exceeded the collapse crater size and agreed well with the spall zone dimension calculated using the seismic parameters from Table 2.

### 2.4 Discussion

In principle, the subsidence measurements could be estimated in millimeter accuracy, but this is hard to achieve in practice, owing to the influence of many errors sources, e.g. atmospheric turbulence, processing approximations, and measurement artifacts etc. In comparison to seismic methods (with about km error ellipse) the reachable accuracy by estimation of horizontal coordinates is obviously better. The selection of the absolute offsets after the phase unwrapping is 'arbitrary', since DInSAR provides relative measures only. However, this is not a critical point if large stable areas are available within the scene. Second, the geologic and hydrologic environment of the local test area is known up to a limited degree only. By lack of information the modeling of deformation is only preliminary. Nevertheless, the results for the derived decay constants and initial deformation rates did not show many regional distinctions. If the measured signals are taken in close time intervals, a 'continuous' time series is obtained. This technology is regarded a valuable tool to

supplement existing methods for monitoring compliance with the CTBT.

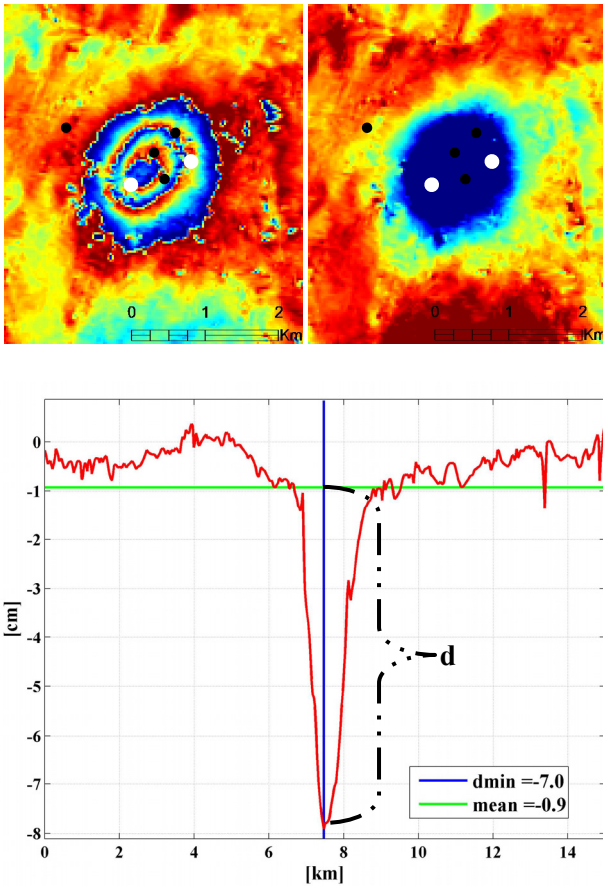


Figure 6. (Top, left) differential interferogram for search area Junction; (top, right) displacement map for the same area. Black and white dots indicate known locations of underground tests before and after 1988, respectively; (bottom) vertical profile across the motion centre with west-east orientation.

### 3. CONCLUSIONS

In comparison to optical EO data SAR is independent from weather conditions and time of day. The differential InSAR techniques offer the opportunity to reveal both coseismic and postseismic subsidence signals caused by underground nuclear explosions with multi-dimensional parameters. Different time-scales of the deformation processes such as long-term and short-time subsidence could be detected by various combinations of the available scenes. These observations seem to open the possibility that InSAR may provide additional capabilities to supplement existing methods for monitoring compliance with the CTBT. We intend to extend this promising NTS observations to other known nuclear test sites investigated so far mostly by seismic methods.

### 4. REFERENCES

Canty, M. J., Nielsen, A. A., Schlittenhardt, J., 2005, Sensitive change detection for remote monitoring of nuclear Treaties. In: *Proceedings of the 31st International Symposium on Remote Sensing of Environment, Global Monitoring for Sustainability and Security*, St. Petersburg, Russia, 20-24 June 2005

Canty, M. J., Schlittenhardt, J., 2001. Satellite data used to locate site of 1998 Indian nuclear test. *EOS Transaction American Geophysical Union*, 82(3), pp. 25-29.

Gabriel, A. K., Goldstein, R. M., Zebker, H. A., 1989, Mapping small elevation changes over large areas: differential radar Interferometry. *Journal of Geophysical research*, 94 (B7), pp. 9183-9191

Gutjahr KH., 2004. Monitoring of Alpine Glaciers via Multipass Differential SAR Interferometry. In: *Proceedings of EUSAR 2004*, pp. 75 – 78, 25-27 May 2004, Ulm

Springer, D. L., Pawloski G.A., Ricca, J. L., Rohrer, R. F., Smith, D. K., 2002. Seismic Source Summary for All U.S. Below-Surface Nuclear Explosions. In: *Bulletin of the Seismological Society of America*, Vol. 92, No. 5, pp. 1806-1840.

Vincent, P., S. Larsen, D. Galloway, R.J. Lacznia, W.R. Walter, W. Foxall, and J. J. Zucca., 2003. New signatures of underground nuclear tests revealed by satellite radar Interferometry. *Geophys. Res Letters*, 30(22), 2141.